Sensitivity Dependence of Single Nanoparticle Mass Detection Using Mechanical Oscillations in Optical Microcavities

Jiancong Li, Xiao-Chong Yu, Yanyan Zhi, Jie Li, and Bai-Ou Guan

***Abstract*—Single nanoparticle detection is demanding in fields such as early-stage diagnostics, environmental monitoring and biochemical researches. Microcavities are becoming excellent platforms for ultrasensitive detection due to the extremely strong enhancement of light-matter interactions. However, the analytes to be detected will introduce optical losses, which eventually spoils the detection limit of the optical sensor. The strong light confinement enables optical induced mechanical oscillations that is also sensitive to analyte attachments and can thus be applied as an alternative sensing signal in microcavity sensors. In this work, the mass sensitivities of the mechanical oscillations of a microcavity are theoretically discussed. The sensitivity dependence on different modes, analyte sensing position and microcavity structure are explored via finite-element-method simulations, which are consistent with theoretical predictions. Our results provide an effective guideline for the sensitivity optimization during microcavity design aiming for single nanoparticle mass detection.**

***Index Terms*—Microsensors, cavity resonators, position sensitive particle detectors.**

I. Introduction

OPTICAL whispering-gallery-mode (WGM) microcavities have been widely applied in sensing applications with detection limit down to single nanoparticles [1]–[5], which is critical in environmental monitoring [6] and early-stage diagnostics [7]. While strong light-matter interactions due to ultra-high quality factors (Q factors) and small mode volumes [8] significantly enhance the sensitivity, the analytes (e.g., nanoparticles) induced scattering and absorption losses degrade Q factor during the detection process [7]. The minimal detectable optical resonance shift, i.e., the optical sensing resolution, is thus enlarged, spoiling the detection limit. Note that a lower detection limit indicates the sensor capability of detecting smaller analytes [9]. Furthermore, the sensing activity only happens when analytes enter the optical mode field which is limited to hundreds of $\mu\mathrm{m}^3$ [10]. The microcavity inevitably loses the sensing capability when the mode shift cannot be resolved or the optical mode area is fully covered by the analyte nanoparticles. Therefore, pursuing alternative sensing signals that do not critically rely on optical resonances open avenues for enhancement of microcavity sensing performances.

The radiation pressure of the strongly confined optical mode field results in the variation of the mechanical rigidity of the microcavity material, known as the optical spring effect (OSE) [11]–[13], which can be utilized as an excellent sensing signal. The frequency of the optomechanical oscillations can be expressed by $\Omega_{\mathrm{m}} = \sqrt{(k_0 + k_{\mathrm{os}})/m_{\mathrm{eff}}}$, where Ω_{m} is the angular frequency of mechanical oscillations, k_0 and k_{os} denote the intrinsic mechanical spring coefficient and optical spring coefficient, respectively, and m_{eff} indicates the effective mass of the cavity [14]–[16]. Single nanoparticle detections have been realized by tracking the mechanical frequency shifts induced by optical mode frequency shifts due to particle attachments on the cavity surface [17], and a noise suppression technique has been demonstrated to reach a better detection limit [18]. In Refs. [17] and [18], the shift of the angular mechanical frequency Ω_{m} is dominantly determined by the change on k_{os} dependent on the intra-cavity power, so that the sensing performance, for example, the sensing resolution and the sensing area, is still limited by the Q factor degradation and small optical mode volume during the detection process.

When the sensing signal does not rely on the light-matter interaction, the loss of the optical mode can be avoided and the Q factor can be preserved. Fortunately, the mechanical frequency, $f_{\mathrm{m}} = \Omega_{\mathrm{m}}/(2\pi)$, is not only a function of k_{os} dependent on optical mode detuning, but also a function of m_{eff}. The effective mass of the microcavity can be express by $m_{\mathrm{eff}} = 2E_{\mathrm{m}}/(r_{\max}^2\Omega_{\mathrm{m}}^2)$, where E_{m} is the total mechanical energy stored in the mechanical mode and $r_{\max}$ denotes the amplitude of the mechanical displacement [11], [13], [19]. The attachments of analytes on the microcavity surface alter m_{eff}, even when the analytes are placed out of the optical mode region. The

Manuscript received June 19, 2021; revised August 4, 2021; accepted August 11, 2021. Date of publication August 18, 2021; date of current version September 6, 2021. This work was supported in part by the National Natural Science Foundation of China under Grant 61805103 and in part by the Local Innovative and Research Teams Project of Guangdong Pearl River Talents Program under Grant 2019BT02X105. The work of Jie Li was supported by the Youth Top-notch Scientific and Technological Innovation Talent of Guangdong Special Support Plan under Grant 2019TQ05X136. The work of Xiao-Chong Yu was supported by the Fundamental Research Funds for the Central Universities under Grant 2019NTST31. *(Corresponding author: Yanyan Zhi.)*

Jiancong Li, Yanyan Zhi, Jie Li, and Bai-Ou Guan are with the Guangdong Provincial Key Laboratory of Optical Fiber Sensing and Communications, Institute of Photonics Technology, Jinan University, Guangzhou 510632, China (e-mail: gzyljc18@stu2019.jnu.edu.cn; yanyanzhi@jnu.edu.cn; tjieli@jnu.edu.cn; tguanbo@jnu.edu.cn).

Xiao-Chong Yu is with the Department of Physics and Applied Optics Beijing Area Major Laboratory, Beijing Normal University, Beijing 100875, China (e-mail: yuxc@bnu.edu.cn).

Color versions of one or more figures in this article are available at https://doi.org/10.1109/JSTQE.2021.3105132.

Digital Object Identifier 10.1109/JSTQE.2021.3105132

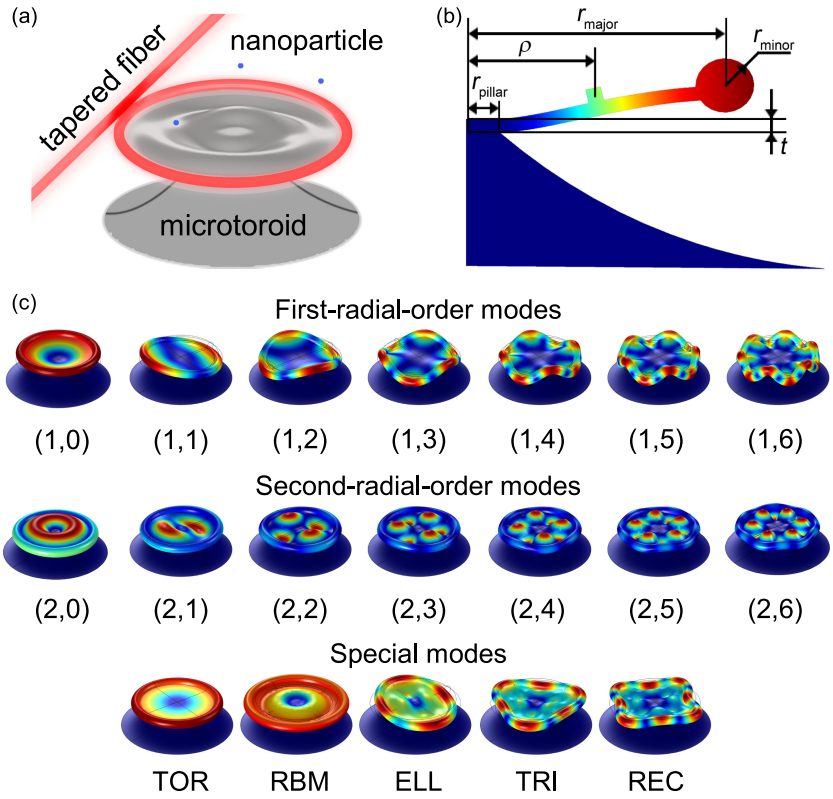

Fig. 1. (a) The schematic of how mechanical oscillations are excited in a high-Q toroidal microcavity. Light in a tapered fiber waveguide is coupled into the WGM of the microcavity via the evanescent field (in red), which then excites the mechanical mode (ripples). (b) The cross-section of one mechanical mode simulated by FEM. (c) First-radial-order, second-radial-order, and special mechanical modes calculated via FEM simulations.

mechanical frequency shift, as the sensing signal, can thus be empolyed to detect analytes without degrading the optical Q factor. Furthermore, when utilizing mechanical oscillations as sensing signals, the sensing area can be significantly enlarged, compared to the case when employing optical modes with small mode volumes. In this work, using the mechanical mode as the sensing signal, the sensitivitis dependent on the structural parameters of a toroidal microcavity and the position of the detection sites are discussed, providing knowledge for obtaining a better detection limit and guiding the design process of a microcavity optomechanical mass sensor.

II. Microcavity Design and Simulation Model

The schematic of exciting mechanical oscillations of a whispering-gallery-mode toroidal microcavity is illustrated in Fig. 1(a). We propose to use a toroidal microcavity, because the on-chip resonator is ready for parallel processing and compatible integration [8]. The number of supported optical modes in a microtoroid is reduced compared to that in a spherical microcavity [20], so that the mode-locking is easier to be maintained, which is necessary to obtain a stable frequency spectrum via a basic spectrum analyzer for analyzing mechanical modes [18]. Furthermore, compared to a microsphere with an equal diameter, the optical mode volume is smaller by a factor of about 5, because the optical mode is tightly confined in the torus [21]. Fig. 1(b) shows the cross-sectional mechanical oscillations of one mechanical mode with $f_{\mathrm{m}} = 1.4$ MHz simulated via finite-element-method (FEM) simulation.

When an analyte nanoparticle attaches on the microcavity surface, the frequency of the mechanical mode shifts, acting as the sensing signal. The nanoparticles are placed out of the optical mode field to avoid the degradation of the Q factor. Note that the variation of the quality factor of the mechanical mode (Q_{m}) induced by analyte attachments, defined as $Q_{\mathrm{m}} = f_{\mathrm{m}}/\delta f_{\mathrm{m}}$ (δf_{m} is the full-width-half-maximum of the mechanical mode), could also act as an alternative sensing signal [16], of which the discussion will not be included in the current proposal.

The frequency shift of mechanical oscillations is applied for mass detection of single nanoparticles in this work. The sensitivity is defined by,

$$S = \Delta f_{\mathrm{m}}/m_{\mathrm{p}} \approx -f_{\mathrm{m}}\delta_p^2/2m_{\mathrm{eff}} \tag{1}$$

where Δf_{m} is the frequency shift of the mechanical mode, m_{p} denotes the mass of the analyte nanoparticle, and δ_p is the relative displacement at the analyte position compared with the displacement maximum $r_{\max}$. When discussing the sensitivity, one usually refers to the magnitude of S, i.e., $|S|$, and the positive/negative sign of S correspond to a blue/red frequency shift. Obviously, a larger mechanical frequency, smaller effective mass and proper analyte position result in a higher sensitivity. In order to optimize the sensing performance of the microcavity, the sensitivity dependence on the following parameters are explored, i) the radial position where the nanoparticle locates ρ, ii) the

microcavity structural parameters including the major radius r_{major}, the minor radius r_{minor}, the top-pillar radius r_{pillar}, and the cavity thickness t (see Fig. 1(b)).

In the theoretical model, we consider the sensitivity dependence of mechanical modes categorized in three groups as shown in Fig. 1(c). Two groups of modes are characterized by the radial and azimuthal mode numbers (n, l), where n indicates the number of oscillation maxima in the radial direction, and $2l$ is the number of wave nodes in the azimuthal direction [11]. For example, modes characterized by (1,0) and (2,0) correspond to the first two rotationally symmetric radial modes. The first-radial-order modes of $(n = 1, l)$ are also named as the crown modes. Some special modes mainly oscillating within the equator plane can also be excited, for example, torsional mode (TOR), radial breathing mode (RBM), ellipse mode (ELL), triangle mode (TRI) and rectangle mode (REC). The RBM experimentally shows the strongest optomechanical coupling due to the strongest modulation of the optical periphery [22]. The mechanical frequency shifts and sensitivities of those modes are calculated when the diameter of single polystyrene (PS) nanoparticle with a density of 1050 $\mathrm{kg/m^3}$ varies from 20 nm to 1000 nm.

The structural parameters of the microcavity are set as: the major radius $r_{\mathrm{major}} = 36$ μm, the minor radius $r_{\mathrm{minor}} = 4$ μm, the top-pillar radius $r_{\mathrm{pillar}} = 5$ μm, and the disk thickness $t = 2$ μm. We consider the sensing areas as the region out of the torus and out of the region on top of the pillar, i,e., the disk area subtracting the area on top of the pillar, so that the Q factor of the optical mode can be preserved during the sensing activities. Nanoparticles with different masses altered by the particle diameters are placed at the radial position of $\rho = 18.5$ μm.

III. Results and Discussions

A. Frequency Shifts of Different Modes

The frequency of the mechanical mode shifts when placing a single nanoparticle on the surface of the microcavity due to the change of the effective mass of the mechanical oscillator. The relative frequency shifts of the first-radial-order, the second-radial-order, and five special modes are shown in Fig. 2(a-c). By linear fitting the relationship of the frequency shift and the nanoparticle mass, the sensitivities are obtained and compared.

Among the mode group with the same radial mode number, the magnitude of the sensitivity is larger for the mode with a higher azimuthal mode number, except that $|S_{(1,0)}|$ is slightly larger than $|S_{(1,1)}|$ due to a higher mechanical frequency (see the inset of Fig. 2(a)). In the first-radial-order group, the mechanical frequency is nearly proportional to l^2, consistent with the vibration of a thin plate. While the effective masses of modes $(1, l \geq 1)$ are similar, $|S_{(1,l)}|$ shows a quadratic dependence on the azimuthal mode number (Fig. 2(d)).

The mode group $(2, l)$ shows better sensing performance than the mode group $(1, l)$ does due to a relatively smaller effective mass and a higher oscillation frequency (Fig. 2(d)), and the mechanical oscillations of the former nearly match with the sensing area. For example, when the azimuthal mode number $l = 1$, the second-radial-order mode is ~ 480 times more

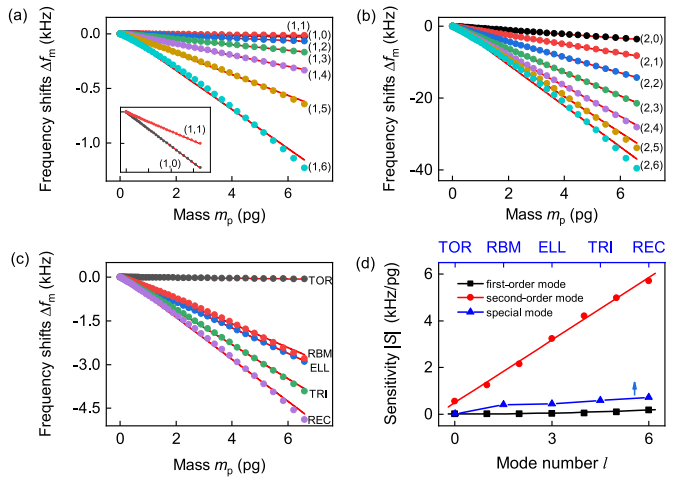

Fig. 2. Frequency shifts of (a) the first-radial-order, (b) the second-radial-order, and (c) special mechanical modes, when placing single nanoparticles with different masses at $\rho = 18.5$ μm. The inset in (a) shows details of the frequency shifts of the modes (1,0) and (1,1). The solid lines in (a)–(c) show the linear fittings. (d) The sensitivities of the three groups of mechanical modes. The sensitivity dependence of the first- and second-radial-order modes are fitted quadratically and linearly respectively. The solid line connecting the special mode data is a guided line.

sensitive than the first-radial-order mode. Compared to that of the first-radial-order mode, the mechanical frequency and the azimuthal mode number also have a quadratic relationship, i.e., $f_{\mathrm{m}} \propto l^2$. Fig. 2(d) shows that $|S_{(2,l)}|$ and l has a nearly linear dependence, i.e., $|S_{(2,l)}| \propto l$.

The sensitivity magnitude of the five special modes is smaller than that of the second-radial-order modes. When comparing to that of the first-radial-order modes, except that the sensitivity of the TOR mode is similar to that of the mode (1,2), the sensitivities of the RBM, ELL, TRI and REC modes are a few times to two orders of magnitude larger than that of the first-radial-order modes, still owing to a higher mechanical frequency. Especially, the RBM shows the strongest optomechanical coupling [22], and is thus used when the excitation power is limited to a lower value to avoid photo-damage, for example, in biological sensing applications. In comparison, a higher-radial-order mode are used when the sensitivity is a critical factor in the sensing performance.

B. Sensitivity Dependence on Sensing Sites

When a single nanoparticle is moved along the radial direction, the frequency shift of the mechanical mode depends on the radial position ρ. When the nanoparticles are placed at the radial position of $\rho = 0 \sim 30$ μm, the magnitudes of the sensitivities of the first- and second-radial-order modes with the same azimuthal mode number $(l = 3)$ are calculated and shown in Fig. 3. The radial position larger than 30 μm is not considered, because the analyte close to the torus has the risk of spoiling the optical Q factor. As predicted by Equation (1), the sensitivity is proportional to the square of the relative displacement in both cases. When the nanoparticle locates on the radial position above the top-pillar region ($r_{\mathrm{pillar}} = 5$ μm), the

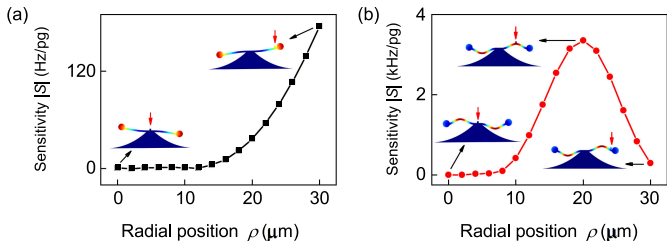

Fig. 3. The sensitivity magnitudes of (a) the first-radial-order (1,3) and (b) the second-radial-order (2,3) modes, when the nanoparticle is placed along different radial positions of $\rho = 0 \sim 30$ μm. The insets show cross-sections of the mechanical oscillations when the nanoparticle, pointed by the red arrows, locates at different radial positions.

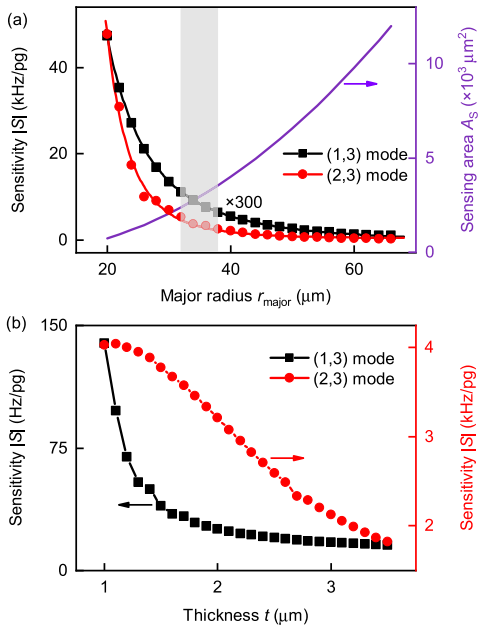

Fig. 4. The sensitivity magnitude dependence of the first-radial-order mode (1,3) and the second-radial-order mode (2,3) on (a) the disk radius and (b) the disk thickness. The black and red curves are the purely third-order and fourth-order polynominal fittings of the sensitivity dependence on r_{major}. The purple curve shows the sensing area as a function of r_{major}.

sensitivity is close to zero, because the mechanical oscillations are almost negligible. When the nanoparticle moves towards the torus, i.e., ρ increases, it enters the region showing mechanical oscillations. Therefore, the magnitude of the sensitivity of mode (1,3) monotonically increases, and $|S_{1,3}| = 175.6$ Hz/pg when $\rho = 30$ μm (Fig. 3(a)). As for the mode (2,3), the sensitivity reaches the maximum of 3.4 kHz/pg at $\rho = 20$ μm, where the peak displacement locates (Fig. 3(b)). When the radial position continues to increase, the sensitivity decreases as the oscillation displacement decreases.

C. Sensitivity Dependence on the Microcavity Dimensions

Next, we explore the sensitivity dependence on the microcavity dimensions, which consists of three parts, the disk region, the torus region, and the pillar region. The nanoparticle is placed at the center between the edges of the pillar and the torus, for example, when $r_{\mathrm{major}} = 30$ μm, $\rho = 15.5$ μm.

1) Disk Radius and Thickness: As the disk radius, r_{major}, scales down, the sensitivity increases, which is similar as the cases of micro-membranes and micro-cantilevers [23], [24]. According to the bending vibration equation, the mechanical frequency is inversely proportional to the square of the scale. As the disk radius increases, the effective mass of the first-radial-order mode is approximately linearly proportional to the radius, i.e., $m_{\mathrm{eff},(1,l)} \propto r_{\mathrm{major}}$, while $m_{\mathrm{eff},(2,l)} \propto r_{\mathrm{major}}^2$. Because $|S| \approx f_{\mathrm{m}}\delta_p^2/(2m_{\mathrm{eff}})$, the sensitivity dependence on the azimuthal number is fitted via $|S_{(1,l)}| \propto r_{\mathrm{major}}^{-3}$ and $|S_{(2,l)}| \propto (r_{\mathrm{major}} - b)^{-4}$, as shown in Fig. 4(a). The fitting parameter b is used in the case of the second-radial-order mode, because the mechanical oscillations are more likely perturbed by the top-pillar, while that of the first-radial-order mode mainly appear in the torus.

However, the sensing area also shrinks quadratically as r_{major} decreases (Fig. 4(a)). The sensitivity magnitude of the second-radial-order mode (2,3) is still up to two orders of magnitude higher than that of the first-radial-order mode (1,3), as discussed in Section III-A. When r_{major} increases from 20 μm to 66 μm, $|S_{(1,3)}|$ ($|S_{(2,3)}|$) decreases by one (two) order of magnitude, while the sensing area enlarges parabolically by about 16 times. The grey-shaded region in Fig. 4(a) indicates trade-off disk dimensions with r_{major} around $32 \sim 38$ μm, which shows both relatively large sensitivities ($|S_{(1,3)}| \approx 30.0$ Hz/pg, $|S_{(2,3)}| \approx 3.5$ kHz/pg) and sensing areas ($A_{\mathrm{s}} \approx 3500$ μm^2).

Similarly, the sensitivity magnitude $|S|$ also decreases as the disk thickness t increases (Fig. 4(b)). Especially, $|S_{(1,3)}|$ decreases faster than $|S_{(2,3)}|$. Although the microcavity with a thinner thickness shows a higher sensitivity, a microtoroid with sub-micrometer thickness is fragile. Practically, a thickness of 2 μm is usually applied in a microtoroidal structure [2], [5], [8], [25]. When $t = 2$ μm, $|S_{(1,3)}|$ still have a reasonable value ($|S_{(1,3)}| = 25.4$ Hz/pg), but is two orders of magnitude smaller than $|S_{(2,3)}|$.

2) Torus Radius: The torus radius (also termed as the minor radius, r_{minor} [26]) influences the sensitivities of the first- and second-radial-order modes in different manners (Fig. 5). With increasing r_{minor}, the sensitivity of the mode (1,3) monotonically decreases due to the increase of the effective mass, and $|S_{(1,3)}|$ is almost zero when $r_{\mathrm{minor}} > 14$ μm (Fig. 5(a)).

In comparison, the sensitivity of the mode (2,3) does not monotonically dependent on r_{minor} due to the mode hybridization with the TRI mode (Fig. 5(b)). The mode hybridization results from the asymmetric support of the vertical pillar structure and was also reported in Refs. [27]–[29]. When r_{minor} increases, the frequency of the mode (2,3) decreases, while the TRI mode behaves in the opposite way and crosses the former one at $r_{\mathrm{minor}} \sim 8.5$ μm (Fig. 5(d)). When $r_{\mathrm{minor}} < 2.8$ μm, $|S_{\mathrm{TRI}}|$ is slightly larger than $|S_{(2,3)}|$. With increasing r_{minor}, $|S_{\mathrm{TRI}}|$ decreases dramatically, while $|S_{(2,3)}|$ increases until $r_{\mathrm{minor}} \sim 8.5$ μm at the crossing point (Fig. 5(b)). At this point, the mode (2,3) and TRI mode hybridize, and the FEM simulation of the mechanical oscillations is shown in Fig. 5(c). After the crossing point, $|S_{(2,3)}|$ and $|S_{\mathrm{TRI}}|$ follow the previous dependence on r_{minor}.

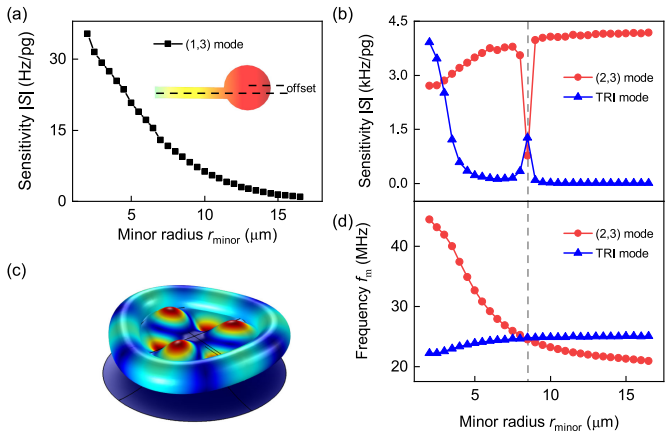

Fig. 5. (a) The sensitivity dependence of the mode (1,3) on the minor radius. The inset shows the position offset between the disk and the torus. (b) The sensitivity dependence of the mode (2,3) (red circles) and TRI mode (blue triangles) on the minor radius. (c) The mechanical oscillations showing the mode hybridization of the mode (2,3) and TRI mode. (d) The frequency dependence of the mode (2,3) (red circles) and TRI mode (blue triangles) on the minor radius.

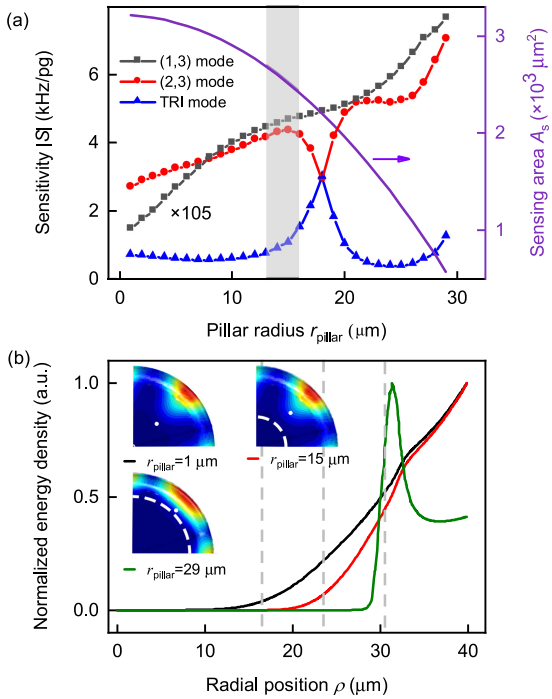

Fig. 6. The sensitivity magnitude dependence of the mode (1,3), (2,3) and TRI mode on the radius of the top-pillar. (b) The normalized energy density along the radial distance from the center of the microcavity. The insets show the top-view FEM simulations when $r_{\mathrm{pillar}} = 1$ μm, 15 μm, and 29 μm, respectively. The three dashed vertical grid lines indicate the nanoparticle position. In the insets, the white symbols indicate the positions where the nanoparticle locates, and the white dashed curves indicate the top-pillar dimensions. When $r_{\mathrm{pillar}} = 1$ μm, the top-pillar is too small to be seen in the inset.

Not only the sensitivity is dependent on the torus (minor) radius, the optical quality factor Q is also dependent on r_{minor}. Larger torus reduces the radiation loss and thus leads to a higher Q factor [30]. Moreover, when $r_{\mathrm{major}} > 18$ μm, Q saturates at $r_{\mathrm{minor}} > 2$ μm [30]. Practically, the torus part of a microtoroidal cavity is formed via re-flowing a microdisk cavity using a CO_2 laser [8], so that the minor diameter can be controlled by the dimensions of the disk and the re-flow process. For example, with the condition that the minor radius is larger than the disk thickness, r_{minor} gets larger when extending the period of the re-flow process or repeating the re-flow procedure for multiple times. When $r_{\mathrm{major}} \approx 60$ μm ($r_{\mathrm{major}} \approx 30$ μm) and $t \approx 2$ μm, and the re-flow process is only done for once, the minor radius of the toroidal part is about 3.5 μm [8] (3 μm [18]).

3) Pillar Radius: The sensitivity dependence on the top-pillar dimension is shown in Fig. 6. The bottom of the pillar is integrated to the wafer, and is set as a fixed constraint in the simulation model. Similarly as the nanoparticle arrangement shown in Fig. 4(a), when examining the relationship of the sensitivity and the top-pillar radius, the nanoparticle is placed at the center between the edges of the pillar and the torus. As r_{pillar} increases, the sensitivity increase of the first-radial-order mode (1,3) could be resulted from two reasons, i) the nanoparticle approaches closer to the mechanical oscillations mainly locating around the torus as shown in the insets of Fig. 6(b), which is consistent to the increase of the sensitivity as illustrated in Fig. 3(a), ii) the normalized energy density where the nanoparticle lies is larger, for example, the normalized energy density is 0.04, 0.07 and 0.71 respectively, as shown in Fig. 6(b).

The sensitivity of the second-radial-order mode (2,3) is about two orders of magnitude higher that of the first-radial-order mode (1,3). Unlike $|S_{1,3}|$, $|S_{2,3}|$ is not monotonically dependent on the top-pillar radius (Fig. 6), which is similarly as the sensitivity dependence on the minor radius as shown in Fig. 5(b). The sensitivity dependence curves of the mode (2,3) and the TRI mode coincide with each other around $r_{\mathrm{pillar}} = 18$ μm due to the hybridization of those two modes as discussed in Sec. III-C2. When r_{pillar} increases from 1 to 29 μm, although $|S_{2,3}|$ increases by 2.6 times, the sensing area decreases by 5.6 times (i.e., from 3213.8 to 574.9 μm^2).

Besides the sensitivity, the mechanical quality factor, Q_{m}, is also dependent on the top-pillar dimension. A larger r_{pillar} adds the mechanical loss to the pillar, resulting in a higher oscillation threshold power [14], [19]. Therefore, reducing the pillar diameter is critical for lowering the threshold powers. Practically, techniques of performing extra etching processes has been applied to achieve a smaller pillar [19]. The mode coupling around $r_{\mathrm{pillar}} = 18$ μm may also introduce mechanical clamping losses and spoiling Q_{m} [27]. Therefore, when using the mode as the sensing signal, the pillar radius can be set around $13 \sim 16$ μm (shaded region in Fig. 6) as a trade-off option of the sensing area, the sensitivity and the mechanical quality factor. Experimentally, the pillar radius can also be altered by controlling the time of the etching process, in which part of the silicon wafer is etched away to form the pillar.

The detection limit of the mass sensor is defined by the ratio of the sensitivity and the detection resolution. The frequency uncertainty of mechanical oscillations is lower than 10 Hz reported in Ref. [18]. Taking the frequency uncertainty as the detection resolution, the detection limit is ~ 3 fg, when using the second-radial-order mode (2,3) with a sensitivity of

~ 3.5 kHz/pg. Note that the sensitivity is also dependent on the microcavity material, because the mechanical frequency and the effective mass are dependent on the rigidity and density of the material. For microtoroidal cavity fabricated using different materials or cavity with different shapes (e.g., microbubble [31], [32] and microdisk [33]), the sensitivity optimization can follow similar process proposed in this work.

Experimentally, during the sensing process of a microcavity sensor, the analyte position is usually not controlled. With sufficient sensing activities, statistical analysis can be applied to obtain the analyte information, for example, the analyte size [2], [34]. However, when the analyte quantity is limited and only a limited number of analyte-sensor interactions is attainable, it's critical to control the location of the analyte on the sensing region. The analyte location on the microcavity can be controlled either by a tip [16] or a taper [7] of which the position can be manipulated by precise piezo-controllers. Once the position of the analyte on the sensor is defined, the analyte mass is possible to be detected by monitoring the mechanical shift.

IV. Conclusion

Mechanical oscillations of a microcavity can be excited via optical spring effect due to ultra-high light confinement, which can act as sensing signals to detect the mass of single nanoparticles. In this work, we explore the sensitivity dependence of mechanical modes on different cavity modes, the sensing sites, and the microcavity structures. Comparing to modes in the first-radial-order group that are relatively easier to be excited, the sensitivity magnitude of the mode with a higher radial order is two orders of magnitude larger. When the modes are in the same radial-order group, the sensitivity magnitude $|S|$ also increases with higher azimuthal mode number. The TOR mode has a similar sensitivity to the fundamental modes, while the RBM, ELL, TRI and REC modes are a few times to over two orders of magnitude more sensitive. The sensitivity is highly dependent on the locations of the nanoparticles, and reaches maximum at the oscillation-peak position.

During the sensitivity optimization process, the sensitivity, the sensing area, and the robustness of the device are considered. The microcavity dimensions determine both the sensitivity and the sensing area. Although a thinner disk thickness results in a higher sensitivity, the microcavity becomes fragile, so the disk thickness is usually around 2 μm. When the major diameter increases, the sensing area enlarges quadratically, while the sensitivity magnitude decreases rapidly, so the major diameter is suggested to be around 35 μm as a trade-off of the sensitivity and the sensing area. When the minor (top-pillar) radius increases, the sensitivity magnitude of the first-radial-order mode monotonically decreases (increases). The mode hybridization of the second-radial-order mode and one of the special modes appears when the minor radius or the top-pillar radius is set at certain values, which degrades the quality factor of the mechanical modes. Especially, the increase of the pillar dimension quadratically shrinks the sensing area. Therefore, trade-off values need to be carefully chosen when designing the microcavity. The knowledge of the sensitivity dependence is essential when the microcavity is used for mass sensing applications, and provides a way for optimizing the detection limit when designing a microcavity sensor.

IV. Contributions

Jiancong Li and X.-C. Yu contribute equally to the work. Y. Zhi conceived the idea and led the project. Jiancong Li and X.-C. Yu conducted the simulation. All authors analyzed the data and wrote the manuscript.

Acknowledgment

The authors would like to thank Jianping Yao from University of Ottawa for helpful discussions.

References

[1] F. Vollmer, S. Arnold, and D. Keng, "Single virus detection from the reactive shift of a whispering-gallery mode," *Proc. Nat. Acad. Sci.*, vol. 105, no. 52, pp. 20 701–20 704, 2008.
[2] J. Zhu *et al.*, "On-chip single nanoparticle detection and sizing by mode splitting in an ultrahigh-Q microresonator," *Nat. Photon.*, vol. 4, no. 1, pp. 46–49, 2010.
[3] S. I. Shopova, R. Rajmangal, S. Holler, and S. Arnold, "Plasmonic enhancement of a whispering-gallery-mode biosensor for single nanoparticle detection," *Appl. Phys. Lett.*, vol. 98, no. 24, 2011, Art. no. 243104.
[4] J. D. Swaim, J. Knittel, and W. P. Bowen, "Detection of nanoparticles with a frequency locked whispering gallery mode microresonator," *Appl. Phys. Lett.*, vol. 102, no. 18, 2013, Art. no. 183106.
[5] B.-Q. Shen *et al.*, "Detection of single nanoparticles using the dissipative interaction in a high-Q microcavity," *Phys. Rev. Appl.*, vol. 5, no. 2, 2016, Art. no. 024011.
[6] X.-C. Yu *et al.*, "Optically sizing single atmospheric particulates with a 10-nm resolution using a strong evanescent field," *Light: Sci. Appl.*, vol. 7, no. 4, 2018, Art. no. 18003.
[7] L. Shao *et al.*, "Detection of single nanoparticles and lentiviruses using microcavity resonance broadening," *Adv. Mater.*, vol. 25, no. 39, pp. 5616–5620, 2013.
[8] D. K. Armani, T. J. Kippenberg, S. M. Spillane, and K. J. Vahala, "Ultra-high-Q toroid microcavity on a chip," *Nature*, vol. 421, no. 6926, pp. 925–928, 2003.
[9] Y. Zhi, X.-C. Yu, Q. Gong, L. Yang, and Y.-F. Xiao, "Single nanoparticle detection using optical microcavities," *Adv. Mater.*, vol. 29, no. 12, 2017, Art. no. 1604920.
[10] T. J. Kippenberg, S. M. Spillane, and K. J. Vahala, "Demonstration of ultra-high-Q small mode volume toroid microcavities on a chip," *Appl. Phys. Lett.*, vol. 85, no. 25, pp. 6113–6115, 2004.
[11] T. J. Kippenberg, H. Rokhsari, T. Carmon, A. Scherer, and K. J. Vahala, "Analysis of radiation-pressure induced mechanical oscillation of an optical microcavity," *Phys. Rev. Lett.*, vol. 95, no. 3, 2005, Art. no. 033901.
[12] M. Hossein-Zadeh and K. J. Vahala, "Observation of optical spring effect in a microtoroidal optomechanical resonator," *Opt. Lett.*, vol. 32, no. 12, pp. 1611–1613, 2007.
[13] T. J. Kippenberg and K. J. Vahala, "Cavity opto-mechanics," *Opt. Exp.*, vol. 15, no. 25, pp. 17172–17205, 2007.
[14] M. Hossein-Zadeh, H. Rokhsari, A. Hajimiri, and K. J. Vahala, "Characterization of a radiation-pressure-driven micromechanical oscillator," *Phys. Rev. A*, vol. 74, no. 2, 2006, Art. no. 023813.
[15] Z. Chen, X. Wu, L. Liu, and L. Xu, "Optical spring effect in micro-bubble resonators and its application for the effective mass measurement of optomechanical resonant mode," *Sensors*, vol. 17, no. 10, 2017, Art. no. 2256.
[16] F. Liu and M. Hossein-Zadeh, "Mass sensing with optomechanical oscillation," *IEEE Sensors J.*, vol. 13, no. 1, pp. 146–147, Jan. 2013.
[17] W. Yu, W. C. Jiang, Q. Lin, and T. Lu, "Cavity optomechanical spring sensing of single molecules," *Nat. Commun.*, vol. 7, 2016, Art. no. 12311.
[18] Y. Zhi, X.-C. Yu, H.-J. Chen, B.-O. Guan, and Y.-F. Xiao, "Noise suppression of mechanical oscillations in a microcavity for ultrasensitive detection," *Opt. Lett.*, vol. 44, no. 10, pp. 2426–2429, 2019.
[19] M. Hossein-Zadeh and K. J. Vahala, "An optomechanical oscillator on a silicon chip," *IEEE J. Sel. Topics Quantum Electron.*, vol. 16, no. 1, pp. 276–287, Jan./Feb. 2010.

[20] T. Kippenberg, S. Spillane, B. Min, and K. Vahala, "Theoretical and experimental study of stimulated and cascaded Raman scattering in ultrahigh-Q optical microcavities," *IEEE J. Sel. Topics Quantum Electron.*, vol. 10, no. 5, pp. 1219–1228, Sep./Oct. 2004.
[21] X. Jiang, A. J. Qavi, S. H. Huang, and L. Yang, "Whispering gallery microsensors: A review," 2018, *arXiv:1805.00062*.
[22] A. Schliesser, G. Anetsberger, R. Rivière, O. Arcizet, and T. J. Kippenberg, "High-sensitivity monitoring of micromechanical vibration using optical whispering gallery mode resonators," *New J. Phys.*, vol. 10, no. 9, 2008, Art. no. 095015.
[23] X. Lu, Z. Xu, X. Yan, S. Li, W. Ren, and Z. Cheng, "Piezoelectric biosensor platform based on ZnO micro membrane," *Curr. Appl. Phys.*, vol. 11, no. 3, pp. S285–S287, 2011.
[24] P. Joshi, S. Kumar, V. K. Jain, J. Akhtar, and J. Singh, "Distributed MEMS mass-sensor based on piezoelectric resonant micro-cantilevers," *J. Microelectromech. Syst.*, vol. 28, no. 3, pp. 382–389, 2019.
[25] S. Forstner *et al.*, "Ultrasensitive optomechanical magnetometry," *Adv. Mater.*, vol. 26, no. 36, pp. 6348–6353, 2014.
[26] B. Min, L. Yang, and K. Vahala, "Perturbative analytic theory of an ultrahigh-Q toroidal microcavity," *Phys. Rev. A*, vol. 76, no. 10, 2007, Art. no. 013823.
[27] G. Anetsberger, R. Rivière, A. Schliesser, O. Arcizet, and T. J. Kippenberg, "Ultralow-dissipation optomechanical resonators on a chip," *Nature Photon.*, vol. 2, no. 10, pp. 627–633, 2008.
[28] X. Sun, X. Zhang, and H. X. Tang, "High-Q silicon optomechanical microdisk resonators at gigahertz frequencies," *Appl. Phys. Lett.*, vol. 100, no. 17, 2012, Art. no. 173116.
[29] Y. Liu, M. Davançço, V. Aksyuk, and K. Srinivasan, "Electromagnetically induced transparency and wideband wavelength conversion in silicon nitride microdisk optomechanical resonators," *Phys. Rev. Lett.*, vol. 110, 2013, Art. no. 223603.
[30] S. M. Spillane, T. J. Kippenberg, K. J. Vahala, K. W. Goh, E. Wilcut, and H. J. Kimble, "Ultrahigh-Q toroidal microresonators for cavity quantum electrodynamics," *Phys. Rev. A*, vol. 71, no. 10, 2005, Art. no. 013817.
[31] D.-Q. Yang *et al.*, "Operando monitoring transition dynamics of responsive polymer using optofluidic microcavities," *Light: Sci. Appl.*, vol. 10, no. 1, 2021, Art. no. 128.
[32] J. Liao and L. Yang, "Optical whispering-gallery mode barcodes for high-precision and wide-range temperature measurements," *Light: Sci. Appl.*, vol. 10, no. 1, 2021, Art. no. 32.
[33] S.-J. Tang *et al.*, "Laser particles with omnidirectional emission for cell tracking," *Light: Sci. Appl.*, vol. 10, no. 1, 2021, Art. no. 23.
[34] M. Jin *et al.*, "1/f-noise-free optical sensing with an integrated heterodyne interferometer," *Nat. Commun.*, vol. 12, no. 1, 2021, Art. no. 1973.

Jiancong Li is currently working toward the master's degree with the Institute of Photonics Technology, Jinan University, Guangzhou, China.

His main research focuses on enhancing the sensitivity of optical microcavities using mechanical oscillations.

Xiao-Chong Yu received the B.S. and Ph.D. degrees in Physics from Peking University, Beijing, China, in 2012 and 2017, respectively.

From 2017 to 2019, he was a Postdoctoral Fellow with Peking University. He is currently an Assistant Professor with Beijing Normal University, Beijing. His research interests include optical fiber sensing and optical microcavity sensing.

Jie Li received the B.S. degree in Physics and the M.S. degree in Optics from Nankai University, Tianjin, China, in 2000 and 2003, respectively, and the Ph.D. degree in Electronic Engineering from the City University of Hong Kong, Hong Kong, in 2008.

From 2003 to 2004, he was with Chuangnam Company Ltd., Shenzhen, China. From 2008 to 2009, he was a Postdoctoral Researcher with Photonics Research Centre and the Department of Electronic and Information Engineering, The Hong Kong Polytechnic University, Hong Kong. Since 2009, he has been a Professor of Optical Engineering with the Institute of Photonics Technology, Jinan University, Guangzhou, China. His research interests include optical fiber devices and sensors.

Yanyan Zhi received the B.S. degree in Applied Physics from Chongqing University, Chongqing, China, in 2008 and the Ph.D. degree in Condensed Matter Physics from the University of Alberta, Edmonton, AB, Canada, in 2014.

From 2015 to 2017, she was a Postdoctoral Fellow with Peking University, Beijing, China. She is currently an Associate Professor with Jinan University, Guangzhou, China. Her research interests include photonic microcavities and microcavity sensing.

Bai-Ou Guan received the B.Sc. degree in Applied Physics from Sichuan University, Chengdu, China, in 1994, and the M.Sc. and Ph.D. degrees in Optics from Nankai University, Tianjin, China, in 1997 and 2000, respectively.

From 2000 to 2005, he was with the Department of Electrical Engineering, The Hong Kong Polytechnic University, Hong Kong, first as a Research Associate, then as a Postdoctoral Research Fellow. From 2005 to 2009, he was with the School of Physics and Optoelectronic Engineering, Dalian University of Technology, Dalian, China, as a Full Professor. In 2009, he joined Jinan University, Guangzhou, China, where he founded the Institute of Photonics Technology. His current research interests include fiber optic devices and technologies, optical fiber sensors, biomedical photonic sensing and imaging, and microwave photonics.